*Progress In Electromagnetics Research Letters, Vol. 37, 153–165, 2013*

# ULTRA-ELONGATED PHOTONIC NANOJETS GENERATED BY A GRADED-INDEX MICROELLIPSOID

**Chengyang Liu***

Department of Mechanical and Electro-Mechanical Engineering, Tamkang University, New Taipei City, Taiwan

**Abstract**—The detailed analysis of localized elongated photonic nanojets generated by a graded-index microellipsoid is reported. Using high resolution finite-difference time-domain simulation, we have studied the distribution of the electric energy density within and in the vicinity outside a dielectric core-shell microellipsoid. Here we consider dielectric composite microellipsoid consisting of a core and several concentric shells having different types of index grading. It becomes possible to elongate the nanojet abnormally. The latitudinal and longitudinal sizes of a nanojet and its peak intensity depending on the optical contrast variation of shells are numerically investigated. The results may provide a new ultra-microscopy technique for optical detection of natural or artificially introduced nanostructures deeply embedded within biological cells.

## 1. INTRODUCTION

The light scattering from small particles is well described by Mie theory [1]. Mie theory solves Maxwell's equations with a quasi-analytical solution rigorously. In recent years, interest in the spatial distribution of electromagnetic intensity both within and in the near field regions external to microspheres has been growing [2–9]. The photonic nanojets are obtained on the shadow side of a dielectric microsphere under plane wave illumination. The most concern of nanojets is that they have a subwavelength beam waist and propagate over several wavelengths with little divergence. The conventional focusing by an objective lens gives diffraction limited optical spots. Subwavelength optical resolution has become necessary for nanoscale applications. Hence, the direct applications of photonic nanojets for

*Received 19 December 2012, Accepted 25 January 2013, Scheduled 14 February 2013*

* Corresponding author: Chengyang Liu (cyliu@mail.tku.edu.tw).

sensing, metrology, Raman spectroscopy [10], two-photon fluorescence enhancement [11], optical trapping [12], and white-light nanoscope [13] have been discussed.

The key parameters of photonic nanojet formed in the vicinity of homogeneous dielectric microspheres and microcylinders under exposure of optical radiation are studied theoretically and experimentally [4–9]. These studies have shown that the shape and intensity of nanojet depend significantly on the size and optical properties of a generating microsphere. When photonic nanojet is produced by a composite radially inhomogeneous sphere consisting of several concentric shells with different refractive indices, the characteristics of photonic nanojet can be changed significantly. It becomes possible to elongate the nanojet abnormally. Kong et al. investigated the photonic nanojet from 2 μm and 5 μm dielectric spheres consisting of 5 and even more concentric layers illuminated by an optical radiation [14–16]. The refractive index of layers varied from optical denser core to the less-dense outer shell. The radially gradual variation of refractive index under certain conditions allowed the photonic nanojet to be elongated up to about $9\lambda$, where $\lambda$ is the wavelength of incident lightwave. However, the cost for this elongation is the nanojet widening in the transverse dimension and the decrease of its peak intensity. Recently, the super-enhancement of photonic nanojets generated at the shadow side surfaces of core-shell microcylinders illuminated by a plane wave is presented by the author [17]. The intensity enhancement of photonic nanojet depends strongly on the thickness of metal shell. Therefore, it would be critical to reduce the size dependence to improve the detection sensitivity in far field optical systems.

In this paper, we theoretically demonstrate the ultra-elongation of photonic nanojets generated at the shadow side surfaces of a graded-index microellipsoid illuminated by a plane wave. The sizes of these microellipsoids are comparable with the incident wavelength, which rules out geometric optics. We therefore use the finite-difference time-domain (FDTD) method for the core-shell microellipsoid to perform the numerical simulation involved in this study. The distributions of the electric energy density within and in the vicinity outside graded-index microellipsoid are computed. Here we consider dielectric composite microellipsoid consisting of a core and several concentric shells having different types of index grading. It becomes possible to elongate the nanojet abnormally. The latitudinal and longitudinal sizes of a nanojet and its peak intensity depending on the optical contrast variation of shells are numerically investigated. The results may provide a new ultra-microscopy technique for optical detection

of natural or artificially introduced nanostructures deeply embedded within biological cells. Details of the calculations and discussion of the results will be presented in the remainder of the paper.

## 2. NUMERICAL METHOD

The Lorenz-Mie theory is widely used to calculate the spatial distribution of optical fields in the vicinity of a dielectric sphere exposed to optical illumination [18]. In this theory, the total optical field is separated conditionally into the incident, internal, and scattered fields with respect to the sphere. However, the focusing properties of a photonic nanojet are affected by other factors that Mie theory does not take into account. The FDTD method [19] is a powerful, accurate numerical method that permits computer-aided design and simulation of photonic nanojets by microspheres. Recently, we have conducted high resolution FDTD simulations on electro-optical resonant switching in side-coupled waveguide-cavity photonic crystal systems [20]. By using high resolution three-dimensional (3-D) FDTD technique to solve Maxwell's equations, we study the internal and near external field distributions of plane wave illuminated dielectric microellipsoids. In 3-D simulations, the computational domain is a cubic box. Here, $\Delta x$, $\Delta y$, and $\Delta z$ are the lattice space increments in the $x$, $y$, and $z$ coordinate directions, respectively. We used centered finite difference expressions for the space and time derivatives that are both calculated and second-order accurate in the space and time increments. During the process of simulation, a 3-D region of $9\,\mu\text{m} \times 4\,\mu\text{m} \times 4\,\mu\text{m}$ is discretized with uniform mesh. The perfectly matched layer (PML) absorbing boundary condition [21] is used to our FDTD simulations to terminate efficiently the outer boundary of the computational region. A source of the field is set a plane monochromatic wave with unit intensity generated at left boundary of the computational domain. After the convergence check performed by the decrease of the mesh size, the mesh size is set to be 10 nm with PML, which can ensure enough accuracy and high calculation speed. The sampling in time is selected to ensure numerical stability of the algorithm. In an explicit scheme such as the FDTD, the time step $\Delta t$ in the calculation is restricted by the spatial discretization. The time step is determined by the Courant limit:

$$\Delta t \leq 1/c\sqrt{1/(\Delta x)^2 + 1/(\Delta y)^2 + 1/(\Delta z)^2} \tag{1}$$

where $c$ is the speed of the lightwave in medium. Using discrete time and lattices according to Yee algorithm, we can obtain light propagation depending on time. The electromagnetic fields propagated

by the FDTD algorithm are the time domain fields. At each location of the computational domain, they have a form similar to that given in Eq. (2):

$$E_z(x, y) = AW(x, y)\sin(\omega t + \phi_i) \tag{2}$$

where $A$ is the amplitude of the field at particular location, $W$ the lightwave profile, and $\phi_i$ the corresponding phase. However, the values of $A$ and $\phi_i$ are not accessible from the time domain fields.

In order to get the full amplitude and phase information of lightwave, we need the stationary complex fields that correspond to the waveform in Eq. (2). The complex electromagnetic fields are the source of all useful information, such as transmitted and reflected powers, overlap integrals with modal fields. The complex fields are calculated by a real time Fourier transform performed in the last time period of the simulation. The Final complex fields can be visualized at specific planes located properly in the computational domain. The validation of the FDTD computational program has been reported by comparing with the exact solution for the light scattering of the small particles [22]. A more detailed treatment of the FDTD method is given in [19–21].

## 3. MODEL OF THE GRADED-INDEX MICROELLIPSOID

Several papers have been reported for the spatial distributions of the internal and near external electromagnetic fields of plane wave illuminated dielectric microspheres [2–17]. These simulations have shown that high intensity photonic nanojets can exist in both the internal and near external fields along the incident axis. The location and the intensity of these near field nanojets depend on the shape of microsphere and refractive index contrast between the microsphere and its surrounding medium. The photonic nanojet of a multilayer microellipsoid can roughly be described with several parameters displayed in Fig. 1. We consider a micrometer size dielectric elliptical particle consisting of a core with radii $a_0$ and $b_0$ and several concentric shells of equal thickness with radii $a_m$ and $b_m$ ($m = 0$ to $N$). Every layer with a number $m$ is optically homogeneous and is characterized by the refractive index $n_m$. The microellipsoid is surrounded by air medium ($n_s = 1$) and is irradiated by a plane monochromatic lightwave with wavelength $\lambda$. The wave propagates along the $x$-axis and is polarized along $y$-axis. The effective length, maximum intensity, and full-width half-maximum of the photonic nanojet are $L$, $I$, and FWHM, respectively. The length of the nanojet can be increased to several micrometers by radially grading the refractive index of the generating

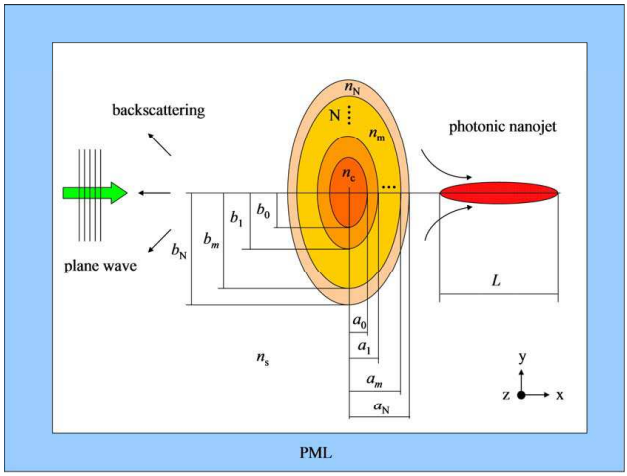


**Figure 1.** Schematic diagram of a multilayer microellipsoid for photonic nanojet.

microellipsoid. To define the refractive index variation from layer to layer, we introduce the refractive index contrast of the graded-index microellipsoid as

$$\frac{n_m}{n_0} = \left(\frac{n_N}{n_0}\right)^{(\frac{m}{N})^g} \tag{3}$$

where $g$ is the index grading type parameter. The $g > 0$ in Eq. (3) specifies the type of refractive index grading starting from the optically densest core and finishing in the outermost shell which has the lowest refractive index. Depending on the $g$ value, it defines linear, concave or convex of index grading. From Eq. (3), the refractive index contrast $C_m$ between neighboring layers is given by the following formula:

$$C_m = \frac{n_m}{n_{m+1}} = \left(\frac{n_0}{n_N}\right)^{\frac{(m+1)^g - m^g}{N^g}} \tag{4}$$

Figure 2 shows the linear ($g = 1$), concave ($g = 0.2$), and convex ($g = 2$) types of refractive index grading at $N = 4$. The refractive index has a maximum value of 1.5 at the core, and decreases in the radial direction to a minimum value of 1.1 at the outer shell. This choice of $n_0$ and $n_N$ values is partly caused by actual possibilities of the modern coating technology of micro-objects with thin shell having variable refractive indices [23–25]. The controlled synthesis of materials with refractive indices in the range 1.05 to 1.9 has been reported by varying the composition and porosity of silica glass. In the present

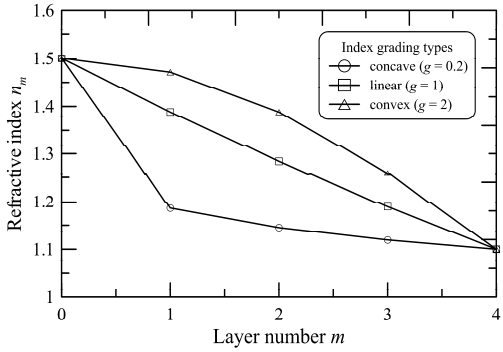


**Figure 2.** Linear ($g = 1$), concave ($g = 0.2$), and convex ($g = 2$) types of refractive index grading at $N = 4$.

work, we consider refractive index grading realized with 4 distinct concentric shells.

## 4. ELONGATED PHOTONIC NANOJET

Several papers show how the length of the photonic nanojet can be increased to several microns by radially grading index of the generating microsphere [14–16]. In conducting the FDTD modeling studies used in this paper, it is found that an even longer and more powerful nanojet could be produced using an alternative radial grading. To study the characteristics of nanojet, it is necessary primarily to define its spatial width and length. The longitudinal profile is obtained as a section of the two-dimensional intensity distribution by the straight line located at $y = 0$, while the transverse profile is obtained as a section by straight line parallel to the $y$ axis and passing through the point of the absolute maximum intensity of nanojet. Fig. 3 shows the normalized intensity distribution of photonic nanojet for dielectric microspheres and microellipsoids along propagation axis ($x$ axis). The all intensities for core-shell microellipsoid are normalized to the intensity for the dielectric microsphere. The radius of microsphere is 1 μm. The microellipsoid has a major axis of 1.5 μm and a minor axis of 0.8165 μm. The two particles have the same volume. The core-shell microellipsoid has a core and 4 concentric shells with different grading index types. The incident wavelength is 532 nm. The core-shell microellipsoid with a smooth gradual drop of the optical contrast between shells ($g = 0.2$) demonstrate longest and low-intensity nanojet with the extent of about $11\lambda$. When the optical contrast between shells increases toward the particle periphery ($g = 2$), the nanojet is barely visible and only a

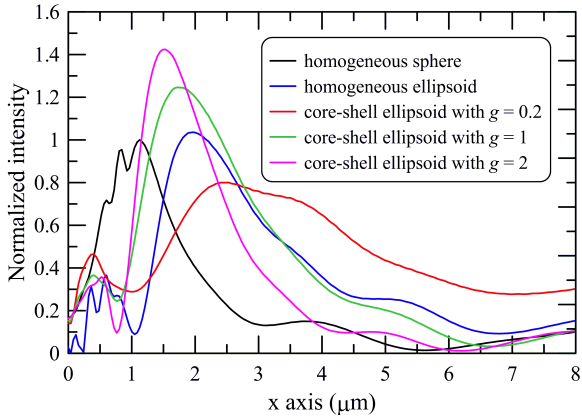


**Figure 3.** Normalized intensity distribution of photonic nanojet for dielectric microspheres and microellipsoids along propagation axis ($x$ axis). The radius of microsphere is 1 μm. The microellipsoid has a major axis of 1.5 μm and a minor axis of 0.8165 μm. The two particles have the same volume. The core-shell microellipsoid has a core and 4 concentric shells with different grading index types. The incident wavelength is 532 nm.

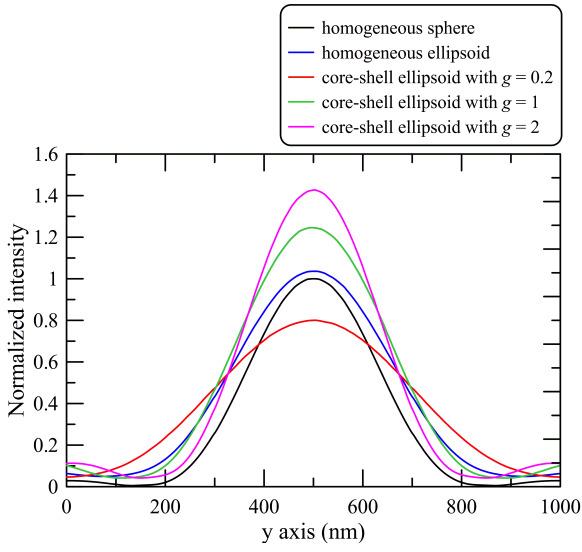


**Figure 4.** Normalized intensity distribution of photonic nanojet for dielectric microspheres and microellipsoids along transversal axis ($y$ axis). The particle designations are the same as in Fig. 3.

ball-like field bunch is formed near the shadow surface. The intensity in this nanojet is several times higher than the maximum nanojet intensity in the spherical case. The nanojet configuration from a particle with the constant interlayer optical contrast ($g = 1$) combines both cases considered above. We can see a high intensity nanojet near the rear hemisphere and a rather long tail. Fig. 4 shows the normalized intensity distribution of photonic nanojet for dielectric microspheres and microellipsoids along transversal axis ($y$ axis). It is important that we have smallest transverse width of nanojet among all considered situations, which does not exceed the incident wavelength.

In order to characterize quantitatively the photonic nanojet, we introduce three parameters: effective length $L$, peak intensity $I$, and full-width half-maximum (FWHM) calculated from the intensity distribution of nanojet. The dependence of these parameters on index grading type parameter $g$ is shown in the series of Fig. 5 to Fig. 7. The nanojet formed in the vicinity of the shadow ellipsoids surface having a decreasing optical contrast ($g < 1$) between shells has the longer effective length, but its peak intensity is low and the FWHM is wide. In core-shell ellipsoids with the optical contrast increasing from the center to the periphery ($g > 1$), the intensity of nanojet is maximal for ellipsoids with the nearly linear variation of the refractive index. In this range of $g$, the FWHM of nanojet has the sub-diffraction size. The effective length $L$ decreases as index grading type parameter $g$ increases. The peak intensity increases as index grading type parameter $g$ increases, and its FWHM to the contrary decreases. Combining basic parameters of nanojet, we propose to characterize the

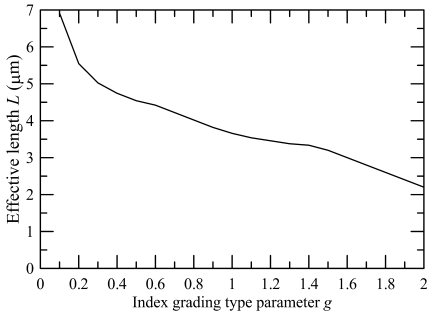


**Figure 5.** Effective length as a function of the index grading type parameter for core-shell microellipsoid.

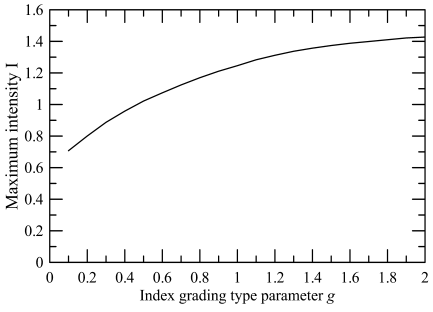


**Figure 6.** Normalized peak intensity as a function of the index grading type parameter for core-shell microellipsoid.

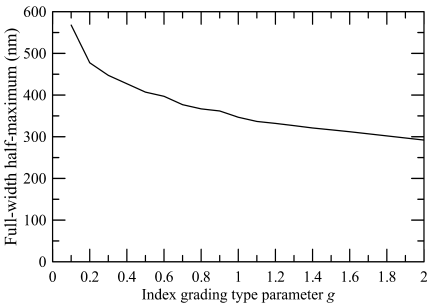


**Figure 7.** Full-width half-maximum of nanojet as a function of the index grading type parameter for core-shell microellipsoid.

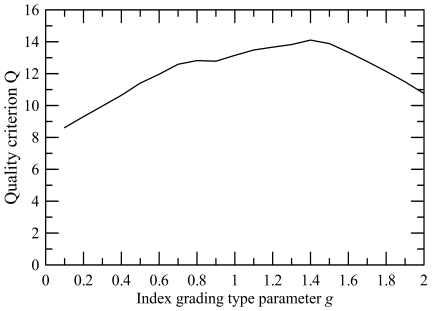


**Figure 8.** Normalized quality criterion of nanojet as a function of the index grading type parameter for core-shell microellipsoid.

photonic nanojet by a quality criterion $Q$ as:

$$Q = \frac{I \times L}{\text{FWHM}} \tag{5}$$

This quality criterion accounts for the utility value of nanojet to the solution of practical problems. When the quality criterion $Q$ is high, the peak intensity of nanojet is high, its FWHM is small, and the effective length is long. Fig. 8 shows the normalized quality criterion of nanojet as a function of the index grading type parameter for core-shell microellipsoid. It turned out that $Q$ possesses the highest value at $g = 1.4$. This morphological type of core-shell ellipsoids optimally combines the high spatial localization of the nanojet with sufficiently high intensity. Fig. 9 shows the normalized electric field intensity distribution of a core-shell microellipsoid at different index grading type parameters. A plane wave at an initial wavelength of 532 nm is incident from the left and impinges on the microellipsoid. Depending on the structural type of ellipsoid, we observe that not only the nanojet dimensions and intensity change but the separation of the nanojet from the ellipsoid surface changes also. At low $g$, the nanojet is formed rather far from the shadow hemisphere, and an increase in $g$ the coordinate of the intensity maximum approaches the ellipsoid rim. At $g > 1$, the nanojet adhered to the outer shell of the ellipsoid and emerges from it in the form of the exponentially decaying trail. In addition, the longitudinal distribution of nanojet becomes more complex. It can be seen from Fig. 9 that a secondary peak appears in the radial direction at a distance of about 1 µm from the principal intensity. This separated light bubble is less intense and its length is smaller than that of the primary nanojet. The optimal balance between

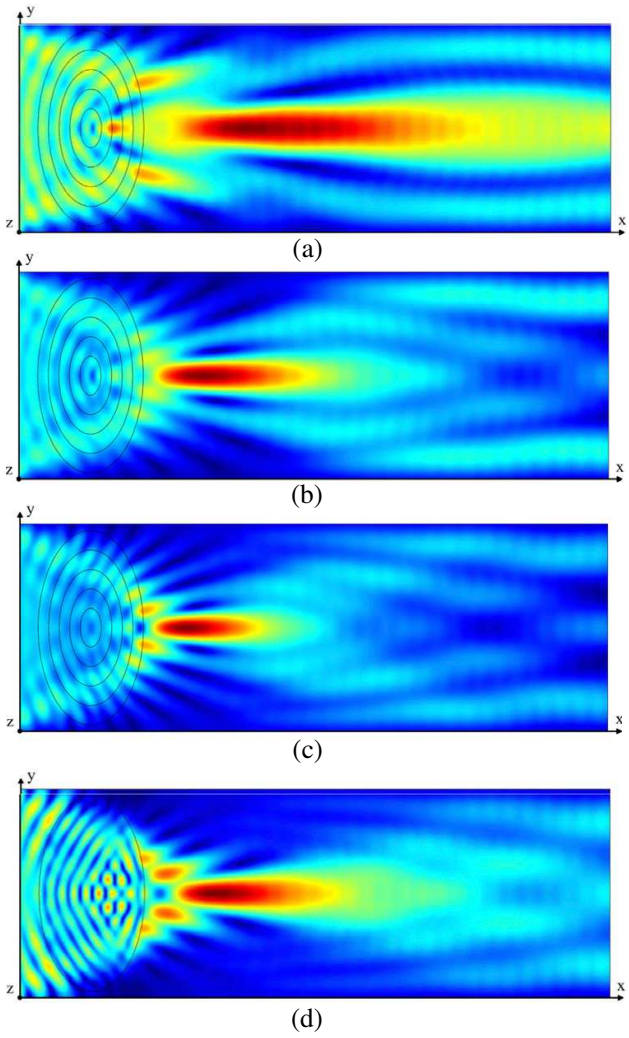


**Figure 9.** Normalized electric field intensity distribution of a core-shell microellipsoid at (a) $g = 0.2$, (b) $g = 1$, (c) $g = 2$, and (d) homogeneous material ($n = 1.5$). Lightwave of wavelength 532 nm propagates from left to right.

the key parameters of nanojet is realized in core-shell ellipsoid with refractive index grading. The incident wavelength of 532 nm is chosen as an example. The photonic nanojet for core-shell ellipsoid is scalable in respect of the incident wavelength.

## 5. CONCLUSION

In conclusion, we have analyzed numerically the ultra-elongation of photonic nanojets generated at the shadow side surfaces of a graded-index microellipsoid illuminated by a plane wave. Using high resolution FDTD simulation, we have considered the basic characteristics (effective length, peak intensity, and FWHM) of nanojets formed in the vicinity of dielectric core-shell ellipsoids with different types of index grading. It is possible to elongate the nanojet abnormally. The latitudinal and longitudinal sizes of a nanojet and its peak intensity depending on the optical contrast variation of shells are numerically investigated. Through the variation of the index grading of shells we can gain control of the nanojet parameters. This mechanism could be an important tool in the fields of nanotechnology and nano-biotechnology. The ultimate phase will test the ability of nanojets to detect nanometer scale features within inhomogeneous objects.

## ACKNOWLEDGMENT

Author acknowledges the financial support from the National Science Council of Taiwan, R.O.C. under Grant No. NSC 101-2221-E-032-009.

## REFERENCES

1. Van de Hulst, H. C., *Light Scattering by Small Particles*, Dover Publications, New York, 1981.
2. Itagi, A. V. and W. A. Challener, "Optics of photonic nanojets," *J. Opt. Soc. Am. A*, Vol. 22, 2847–2858, 2005.
3. Li, C., G. W. Kattawar, and P. Zhai, "Electric and magnetic energy density distributions inside and outside dielectric particles illuminated by a plane electromagnetic wave," *Opt. Express*, Vol. 13, 4554–4559, 2005.
4. Heifetz, A., J. J. Simpson, S. Kong, A. Taflove, and V. Backman, "Subdiffraction optical resolution of a gold nanosphere located within the nanojet of a Mie-resonant dielectric microsphere," *Opt. Express*, Vol. 15, 17334–17342, 2007.
5. Ferrand, P., J. Wenger, A. Devilez, M. Pianta, B. Stout, N. Bonod, E. Popov, and H. Rigneault, "Direct imaging of photonic nanojets," *Opt. Express*, Vol. 16, 6930–6940, 2008.
6. Devilez, A., B. Stout, N. Bonod, and E. Popov, "Spectral analysis of three-dimensional photonic jets," *Opt. Express*, Vol. 16, 14200–14212, 2008.

7. Holms, K., B. Hourahine, and F. Papoff, "Calculation of internal and scattered fields of axisymmetric nanoparticles at any point in space," *J. Opt. A: Pure Appl. Opt.*, Vol. 11, 054009, 2009.
8. Kim, M., T. Scharf, S. Mühlig, C. Rockstuhl, and H. P. Herzig, "Engineering photonic nanojets," *Opt. Express*, Vol. 19, 10206–10220, 2011.
9. Yang, S., A. Taflove, and V. Backman, "Experimental confirmation at visible light wavelengths of the backscattering enhancement phenomenon of the photonic nanojet," *Opt. Express*, Vol. 19, 7084–7093, 2011.
10. Yi, K. J., Y. F. Lu, and Z. Y. Yang, "Enhanced Raman scattering by self-assembled silica spherical microparticles," *J. Appl. Phys.*, Vol. 101, 063528, 2007.
11. Lecler, S., S. Haacke, N. Lecong, O. Crégut, J. Rehspringer, and C. Hirlimann, "Photonic jet driven non-linear optics: Example of two-photon fluorescence enhancement by dielectric microspheres," *Opt. Express*, Vol. 15, 4935–4942, 2007.
12. Cui, X., D. Erni, and C. Hafner, "Optical forces on metallic nanoparticles induced by a photonic nanojet," *Opt. Express*, Vol. 16, 13560–13568, 2008.
13. Wang, Z., W. Guo, L. Li, B. Lukyanchuk, A. Khan, Z. Liu, Z. Chen, and M. Hong, "Optical virtual imaging at 50 nm lateral resolution with a white-light nanoscope," *Nat. Commun.*, Vol. 2, 218, 2011.
14. Kong, S., A. Taflove, and V. Backman, "Quasi one-dimensional light beam generated by a graded-index microsphere," *Opt. Express*, Vol. 17, 3722–3731, 2009.
15. Ruiz, C. and J. J. Simpson, "Detection of embedded ultra-subwavelength-thin dielectric features using elongated photonic nanojets," *Opt. Express*, Vol. 18, 16805–16812, 2010.
16. Geints, Y., E. K. Panina, and A. A. Zemlyanov, "Control over parameters of photonic nanojets of dielectric microspheres," *Opt. Commun.*, Vol. 283, 4775–4781, 2010.
17. Liu, C.-Y., "Superenhanced photonic nanojet by core-shell microcylinders," *Phys. Lett. A*, Vol. 376, 1856–1860, 2012.
18. Bohren, C. F. and D. R. Huffman, *Absorption and Scattering of Light by Samll Particles*, Wiley, New York, 1983.
19. Taflove, A. and S. C. Hagness, *Computational Electrodynamics: The Finite Difference Time Domain Method*, Artech House, Boston, 1998.
20. Liu, C.-Y., "Electro-optical resonant switching in two-dimensional

side-coupled waveguide-cavity photonic crystal systems," *Phys. Lett. A*, Vol. 375, 3895–3898, 2011.

21. Berenger, J.-P., "A perfectly matched layer for the absorption of electromagnetic waves," *J. Comput. Phys.*, Vol. 114, 185–200, 1994.
22. Li, C., G. W. Kattawar, and P. Yang, "Effects of surface roughness on light scattering by small particles," *J. Quant. Spectrosc. Radiat. Transfer*, Vol. 89, 123–131, 2004.
23. Prodan, E., C. Radloff, N. J. Halas, and P. Nordlander, "A hybridization model for the plasmon response of complex nanostructures," *Science*, Vol. 302, 419–422, 2003.
24. Poco, J. F. and L. W. Hrubesh, "Method of producing optical quality glass having a selected refractive index," U.S. Patent 6,158,244, 2008.
25. Mazurin, O. V., M. V. Streltsina, and T. P. Shvaiko-Shavaikovskaya, *Handbook of Glass Data*, Elsevier, Amsterdam, 1993.